An Approach for Elastodynamic Modeling of Hybrid Robots based on Substructure Synthesis Technique

Long Wu[a], Guofeng Wang[a,*], Haitao Liu[a], Tian Huang[a,b]

[a]*Key Lab. of Mechanisms Theory and Equipment Design of the State Education Ministry, Tianjin University, Tianjin 300072, China*
[b]*School of Engineering, The University of Warwick, Coventry CV4 7AL, UK*

Abstract

Parallel kinematic machines exhibit strong pose-dependent static and dynamic behaviors, which makes accurate and rapid compliance analysis over the entire workspace an important issue in the design optimization. This paper presents a general approach for elastodynamic modeling of parallel kinematic machines using substructure synthesis technique. Firstly, the whole system is decomposed into two groups of substructures, i.e. component substructures and joint substructures. Then, the degrees of freedom of component substructures are reduced using modal reduction technique, and joint substructures are modeled by virtual springs with contact stiffness between adjacent component substructures. Finally, two threads are merged at junction surfaces to offer the equations of motion of the system as a whole, allowing the static and dynamic performances to be rapidly predicted with sufficient accuracy. The dynamic model of a 5-DOF hybrid robot is developed using the proposed method and the computational results show that rigidity and lower mode natural frequencies over the workspace match well with those obtained by the full finite element analysis.

Key words: *Substructure synthesis, Modal reduction, Virtual joints, Parallel kinematic machines*

Nomenclature

R	Global reference frame
R^C, R_m^J	Body-fixed frame of component substructure and joint element *m*.
$\boldsymbol{m}$, $\boldsymbol{k}$	Mass and stiffness matrices of a component substructure evaluated in R^C
$\boldsymbol{u}$, $\boldsymbol{f}$	Nodal displacement and force vector of a component substructure evaluated in R^C
$\boldsymbol{u}_j$, $\boldsymbol{u}_i$	Nodal displacement vector of junction nodes and interior nodes evaluated in R^C
$\boldsymbol{m}_R$, $\boldsymbol{k}_R$	Reduced mass and stiffness matrices of a component substructure evaluated in R^C
$\boldsymbol{u}_R$, $\boldsymbol{f}_R$	Reduced nodal displacement and force vector of a component substructure evaluated in R^C
$\boldsymbol{T}_S$	Equivalent static transformation matrix
$\boldsymbol{\Phi}$, $\boldsymbol{I}$	Mode shape matrix and unit matrix
$\boldsymbol{M}^C$, $\boldsymbol{K}^C$	Reduced mass and stiffness matrices of a component substructure evaluated in R
$\boldsymbol{U}^C$, $\boldsymbol{F}^C$	Reduced nodal displacement and force vector of a component substructure evaluated in R
$\boldsymbol{R}_C$	Orientation matrix of R^C with respect to R
$\boldsymbol{T}_C$	Coordinate transformation matrix of R^C with respect to R
$\boldsymbol{k}_m$	Stiffness matrix of joint element *m* evaluated in R_m^J
$\boldsymbol{R}_{J,m}$	Orientation matrix of R_m^J with respect to R
$\boldsymbol{T}_{J,m}$	Adjoint transformation matrix of R_m^J with respect to R
$\boldsymbol{k}^J$	Stiffness matrix of serially connected joint elements evaluated in R
$\boldsymbol{M}^J$, $\boldsymbol{K}^J$	Mass and stiffness matrices of a joint substructure evaluated in R
$\boldsymbol{U}^J$, $\boldsymbol{F}^J$	Nodal displacement and force vector of a joint substructure evaluated in R
$\boldsymbol{U}_i^V$	Nodal displacement vector of virtual node on component substructure C_i
$\boldsymbol{U}_{i,j}^C$	Junction displacement nodal vector of component substructure C_i
$\boldsymbol{U}_{i,p}^C$	Internal elastic modal coordinate vector of component substructure C_i
$\boldsymbol{\varepsilon}_i$, $\boldsymbol{\xi}_i$	Translational and angular nodal displacement vector of virtual node on component substructure C_i
$\boldsymbol{r}_{i,q}$	Position vector pointing from the virtual node to the corresponding junction node *q*
$w_{i,q}$	Weight factor for junction node *q* on component substructure C_i
$\boldsymbol{\lambda}$	Lagrange multipliers

* Corresponding author. Tel./fax: +86 2227406951
E-mail addresses: gfwangmail@tju.edu.cn, (Guofeng. Wang)

$\boldsymbol{C}$ Displacement operator for substructures

1. Introduction

Static and dynamic compliances are two important performance factors of parallel kinematic machines (PKMs) [1-5] especially for those dedicated to metal cutting, high-speed milling or drilling for example, where high rigidity and high dynamics are crucially required. Since static and dynamic behaviors are highly pose-dependent within the work envelop [6-11], the development of effective techniques for dynamic modeling is of great importance in the design optimization as well as in the cutting stability prediction. Literature reveals intensive investigations in the past decades towards dynamic modeling of PKMs. The approaches available at hand can roughly be classified into four categories, i.e., lumped parameter method, semi-analytical method, finite element (FE) method, and substructure synthesis method.

Finite element analysis (FEA) [12-14] is the most accurate method because 3D geometry of links, contact rigidity of joints, and distributed external forces (gravity for example) can be precisely modeled. However, the FE model has to be re-meshed over and over again at different configurations, involving a time consuming procedure. In order to overcome this problem, Ma et al. [15] presented a feature-based CAD-CAE integration method that allows the FE model at different configurations to be updated automatically in a batch manner. The FE model at a given configuration, however, would still have over hundred thousand degrees of freedom, causing a high computational cost in static and dynamic analyses. Therefore, the FE model is more suitable for the final design or validation of other static and dynamic analysis approaches.

In order to improve computational efficiency for static and dynamic behavior prediction in the stage of conceptual design, the lumped spring-mass model could be employed for the systems where the dynamic behaviors are presumably dominated by inertia of the movable components and rigidities of joints. The typical PKM that can be modeled as a lumped spring-mass system would be the Stewart platform. Compared with the lumped parameter method, the semi-analytical methods typically represented by Kineto-Elastodynamics (KED) [16-21] and Flexible Multibody Dynamics (FMD) [22-23] are more suitable for formulating dynamic models of planar and spatial PKMs where the component compliances are no longer negligible. In these methods, the movable links are usually modeled by planar and/or spatial beam elements or finite segments, resulting in either the linear or nonlinear equations of motion, depending upon whether or not taking into the coupling effects of rigid motions over the flexible motions. Generally speaking, the FMD method is more general and effective than the KED method because the constraints imposed by loop closures can be simply modeled by Lagrange multipliers. Along these two tracks, Li et al. [19] developed a dynamic model for the optimal design of a 2-DOF planar parallel robot by maximizing the mean value of the first order natural frequency subject to the prescribed force/motion transmissibility. Piras et al. [20] formulated the dynamic model of a 3-RRR planar parallel mechanism by which the variation of lower natural frequencies with the system configurations were discussed. Zhou et al. [21] studied the vibration problem of a 3-RPS parallel manipulator by treating the joints as virtual springs. Fattah and Angeles [22] investigated the influence of link compliances on the positioning accuracy of a 3-DOF parallel robot, and Wang and Mills [23] discussed the control issue of a 3-PRR flexible planar parallel mechanism. In order to improve the computational efficiency without losing too much accuracy, substructure synthesis or component mode synthesis (CMS) method [24] would be a good choice in dealing with dynamic modeling of mechanical systems that contain movable components (links) having complex geometry. The merit of this method lies in that the number of degrees of freedom (DOF) of a component substructure (link) precisely modeled by FE can significantly be reduced by modal reduction technique while keeping the essential static and dynamic behaviors of the system almost unchanged. The CMS method has been employed, through case-by-case studies, to deal with dynamic modeling of four-bar linkages [25] as well as simple serial or parallel kinematic chains [26]. For example, by taking a two-link serial kinematic chain as an example, Liew et al. [25] proposed a mixed-interface substructure synthesis method for dynamic analysis of multibody systems. In comparison with the results obtained by FEA method, they showed that the computational time can be significantly saved subject to a given accuracy. More recently, Law and Altintas [27] studied dynamic modeling problem of a 5-DOF PKM. They modeled the limbs of the 2-DOF overconstrained planar parallel mechanism by Timoshenko beams while the other components by the modal reduction technique on the basis of the full FE models. This special treatment enables the computational efficiency to be dramatically improved in dynamic behavior prediction over the entire workspace. In view of the previous work mentioned above, a more general methodology is expected for elastodynamic modeling of PKM systems using the CMS technique, and for valid treatment of the joint rigidities since they have great bearings on the static and dynamic characteristics of the system as a whole.

Building upon the substructure synthesis technique, this paper presents a general approach for elastodynamic modeling of PKMs. The major interests will be placed upon the establishment of a modeling framework in general and the specific treatment for rigidity modeling of joints at junction surface by introducing virtual nodes between two adjacent substructures. The remainder of the paper is organized as follows. Having addressed a brief introduction to the dynamic modeling techniques in Section 1, the detailed procedure for dynamic modeling of PKM systems is systematically addressed in Section 2 using modal reduction, virtual joint and substructure synthesis techniques. In Section 3, by taking a newly invented hybrid robot named TriMule [28] as an example, the stiffness and lower mode natural frequencies of the robot are calculated and compared with those obtained by its full FE model, leading to an illustration of the effectiveness of the proposed approach before conclusions are drawn in Section 4.

2. Generalized Method for Dynamic Modeling of Parallel Kinematic Machines

Without loss of generality, consider a PKM comprising a parallel mechanism plus a wrist attached to the platform of the parallel mechanism by a thrust bearing as shown in Fig.1. It can be visualized as an assembly composed of a number flexible multibodies connected by a set of elastic joints in between. Fig.2 shows the overall procedure for dynamic modeling of the PKM using the substructure synthesis method. The first step in the modeling process is to divide the system into two groups of substructures. The first group contains a number of component substructures (C) having relative motions, and the second group contains a number of joint substructures (J) connecting two adjacent component substructures. The second step in the modeling process is to model each component substructure by FEA first and followed by modal reduction technique. Meanwhile, each joint substructure is modeled by the virtual joint method with the stiffness coefficients representing the equivalent contact stiffness between adjacent component substructures. The third step involves transforming the nodal displacements of the reduced models of component substructure evaluated in the body-fixed frame to the global reference frame R attached to the machine frame. Finally, assembling two threads using the compatibility conditions leads to the complete dynamic model of the system. In this way, the static and dynamic behaviors at any configuration can be rapidly evaluated by merely updating the coordinate transformation matrices accordingly. The detailed formulation of the substructure models and synthesis of the equations of motion of the system will be addressed in what follows.

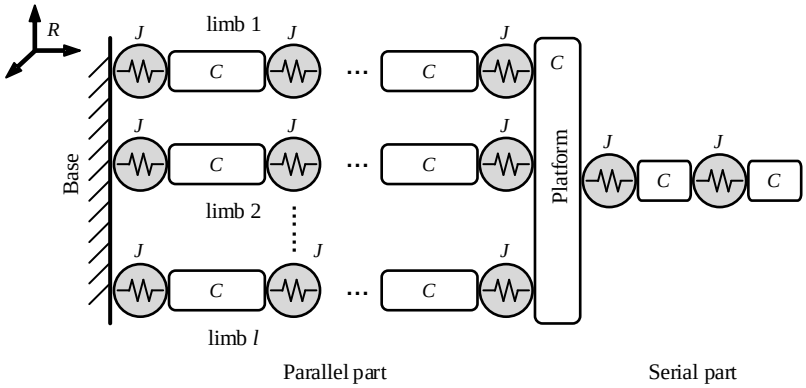

Fig.1 Elastic model of a PKM

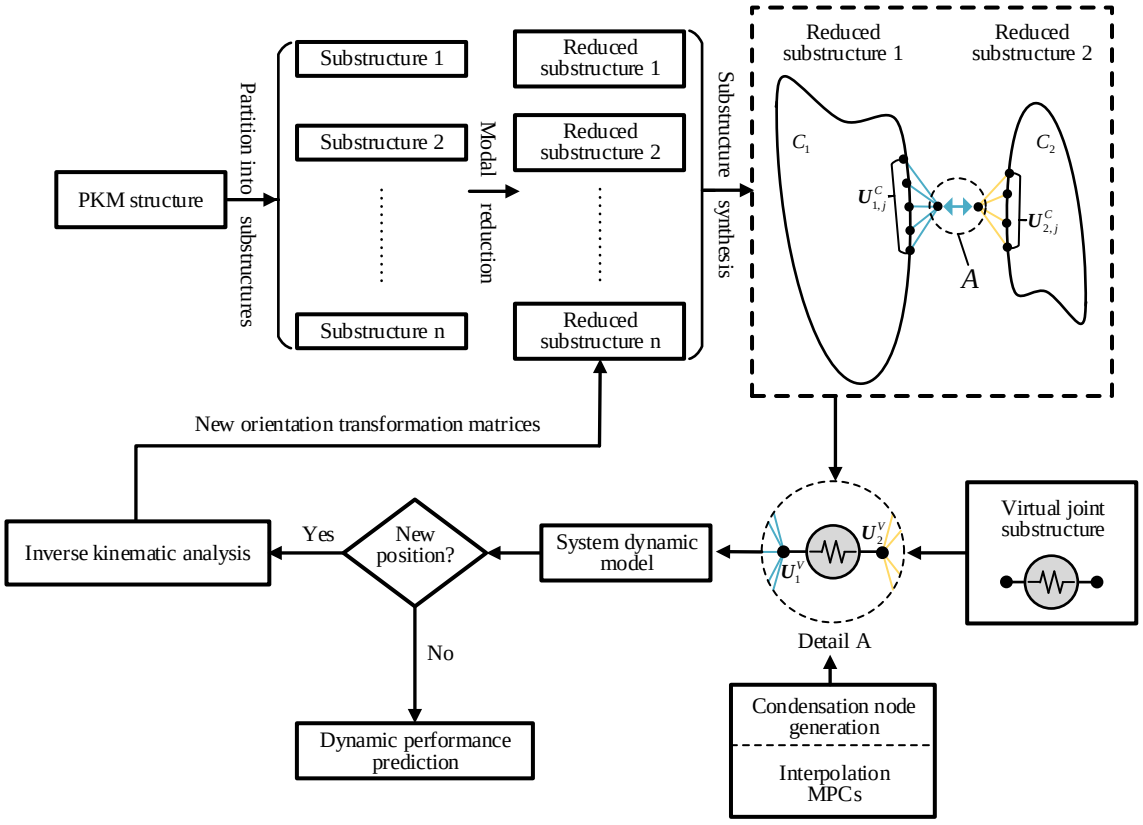

Fig.2 Overview of the proposed modeling scheme

2.1. Modeling of Component Substructures

In this section we will briefly recall the modal reduction technique based upon the constraint-interface synthesis method. Assume that a component substructure is connected with a number of joint substructures as shown in Fig.3. The undamped equation of motion of the component substructure can be created by an FE software in its body-fixed frame R^C

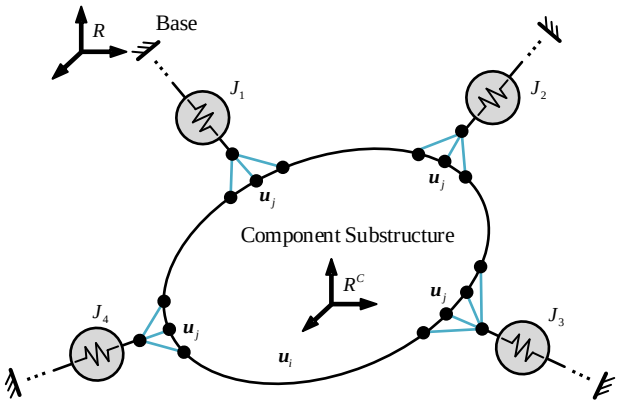

Fig.3 Nodes partition of component substructure

$$\boldsymbol{m}\ddot{\boldsymbol{u}} + \boldsymbol{k}\boldsymbol{u} = \boldsymbol{f} \tag{1}$$

where $\boldsymbol{m}$ and $\boldsymbol{k}$ are the mass and stiffness matrices, $\boldsymbol{u}$ and $\boldsymbol{f}$ are the nodal displacement and force vectors of the full FE model of the component substructure, respectively. In the modal reduction, it is assumed that $\boldsymbol{u}$ can be linearly expressed in terms of a reduced nodal displacement vector $\boldsymbol{u}_R$

$$\boldsymbol{u} = \boldsymbol{T}\boldsymbol{u}_R \tag{2}$$

where $\boldsymbol{T}$ denotes the coordinate transformation matrix from the reduced nodal displacements to the full nodal displacements . Then, substituting Eq.(2) into Eq.(1) leads to the reduced mass and stiffness matrices as well as the nodal force vector of the substructure.

$$\boldsymbol{m}_R = \boldsymbol{T}^{\mathrm{T}}\boldsymbol{m}\boldsymbol{T}\,,\quad \boldsymbol{k}_R = \boldsymbol{T}^{\mathrm{T}}\boldsymbol{k}\boldsymbol{T}\,,\quad \boldsymbol{f}_R = \boldsymbol{T}^{\mathrm{T}}\boldsymbol{f} \tag{3}$$

In order to determine $\boldsymbol{u}_R$ and $\boldsymbol{T}$, partition $\boldsymbol{u}$ into two subsets, i.e. the junction nodal displacement vector $\boldsymbol{u}_j$ and the interior nodal displacement vector $\boldsymbol{u}_i$ as shown in Fig.3 such that

$$\boldsymbol{u} = \begin{pmatrix} \boldsymbol{u}_j \\ \boldsymbol{u}_i \end{pmatrix},\quad \boldsymbol{m} = \begin{bmatrix} \boldsymbol{m}_{jj} & \boldsymbol{m}_{ji} \\ \boldsymbol{m}_{ij} & \boldsymbol{m}_{ii} \end{bmatrix},\quad \boldsymbol{k} = \begin{bmatrix} \boldsymbol{k}_{jj} & \boldsymbol{k}_{ji} \\ \boldsymbol{k}_{ij} & \boldsymbol{k}_{ii} \end{bmatrix},\quad \boldsymbol{f} = \begin{pmatrix} \boldsymbol{f}_j \\ \boldsymbol{0} \end{pmatrix} \tag{4}$$

In the light of the CMS-CB method [29, 30], the interior nodal displacement vector $\boldsymbol{u}_i$ can be approximately expressed as a linear combination of the quasi-static modes and the first p normalized elastic modes. This approximation leads to

$$\begin{pmatrix} \boldsymbol{u}_j \\ \boldsymbol{u}_i \end{pmatrix} = \begin{bmatrix} \boldsymbol{I}_{jj} & \boldsymbol{0}_{jp} \\ \boldsymbol{T}_S & \boldsymbol{\Phi}_{ip} \end{bmatrix} \begin{pmatrix} \boldsymbol{u}_j \\ \boldsymbol{u}_p \end{pmatrix} \tag{5}$$

where $\boldsymbol{u}_p$ is the modal coordinate vector corresponding to the first p elastic modes by locking all DOFs of $\boldsymbol{u}_j$, $\boldsymbol{T}_S = -\boldsymbol{k}_{ii}^{-1}\boldsymbol{k}_{ij}$ is the equivalent static (Guyan) transformation [31], and $\boldsymbol{\Phi}_{ip} \subseteq \boldsymbol{\Phi}_{ii}$ is the modal matrix formed by the first p mode shapes of the constrained system whose full modal matrix $\boldsymbol{\Phi}_{ii}$ can be obtained by solving a generalized eigenvalue problem. In order to improve the accuracy of the approximated quasi-static modes, the Improved Component Mode Synthesis (ICMS) method [32, 33] can be employed to determine $\boldsymbol{T}_S$ using the following iterative formula.

$$\boldsymbol{T}_S^{(k+1)} = -\boldsymbol{k}_{ii}^{-1}\boldsymbol{k}_{ij} + \boldsymbol{k}_{ii}^{-1}\left(\boldsymbol{m}_{ij} + \boldsymbol{m}_{ii}\boldsymbol{T}_S^{(k)}\right)\left(\boldsymbol{m}_S^{(k)}\right)^{-1}\boldsymbol{k}_S^{(k)} \tag{6}$$

$$\boldsymbol{m}_S^{(k)} = \begin{bmatrix} \boldsymbol{I}_{jj} \\ \boldsymbol{T}_S^{(k)} \end{bmatrix}^{\mathrm{T}} \boldsymbol{m} \begin{bmatrix} \boldsymbol{I}_{jj} \\ \boldsymbol{T}_S^{(k)} \end{bmatrix}, \quad \boldsymbol{k}_S^{(k)} = \begin{bmatrix} \boldsymbol{I}_{jj} \\ \boldsymbol{T}_S^{(k)} \end{bmatrix}^{\mathrm{T}} \boldsymbol{k} \begin{bmatrix} \boldsymbol{I}_{jj} \\ \boldsymbol{T}_S^{(k)} \end{bmatrix} \tag{7}$$

where the initial $\boldsymbol{T}_S^{(1)}$ can be determined by

$$\boldsymbol{T}_S^{(1)} = -\boldsymbol{k}_{ii}^{-1}\boldsymbol{k}_{ij} + \boldsymbol{k}_{ii}^{-1}\boldsymbol{m}_{ij} + \boldsymbol{m}_{ii}\left(\boldsymbol{m}_{ij} - \boldsymbol{m}_{ii}\boldsymbol{k}_{ii}^{-1}\boldsymbol{k}_{ij}\right)\boldsymbol{m}_T^{-1}\boldsymbol{k}_T \tag{8}$$

$$\boldsymbol{m}_T = \begin{bmatrix} \boldsymbol{I}_{jj} \\ -\boldsymbol{k}_{ii}^{-1}\boldsymbol{k}_{ij} \end{bmatrix}^{\mathrm{T}} \boldsymbol{m} \begin{bmatrix} \boldsymbol{I}_{jj} \\ -\boldsymbol{k}_{ii}^{-1}\boldsymbol{k}_{ij} \end{bmatrix}, \quad \boldsymbol{k}_T = \begin{bmatrix} \boldsymbol{I}_{jj} \\ -\boldsymbol{k}_{ii}^{-1}\boldsymbol{k}_{ij} \end{bmatrix}^{\mathrm{T}} \boldsymbol{k} \begin{bmatrix} \boldsymbol{I}_{jj} \\ -\boldsymbol{k}_{ii}^{-1}\boldsymbol{k}_{ij} \end{bmatrix} \tag{9}$$

For more information about the ICMS method, please refer to [32, 33].

Having developed the reduced model of the component substructure evaluated in the body-fixed frame R^C, the following coordinate transformation can be made to map the reduced nodal displacements from its body-fixed frame R^C to the global reference frame R.

$$\boldsymbol{U}^C = \boldsymbol{T}_C \boldsymbol{u}_R \tag{10}$$

such that

$$\boldsymbol{M}^C = \boldsymbol{T}_C \boldsymbol{m}_R \boldsymbol{T}_C^{\mathrm{T}}, \quad \boldsymbol{K}^C = \boldsymbol{T}_C \boldsymbol{k}_R \boldsymbol{T}_C^{\mathrm{T}}, \quad \boldsymbol{F}^C = \boldsymbol{T}_C \boldsymbol{f}_R \tag{11}$$

where $\boldsymbol{M}^C$ and $\boldsymbol{K}^C$ are the reduced mass and stiffness matrices, $\boldsymbol{U}^C$ and $\boldsymbol{F}^C$ are the nodal displacement and nodal force vectors of the component substructure evaluated in R; $\boldsymbol{T}_C = \mathrm{diag}\left[\boldsymbol{R}_C, \cdots, \boldsymbol{R}_C\right]$ with $\boldsymbol{R}_C$ being the orientation matrix of R^C with respect to R, which can be obtained by inverse kinematics at a given pose of the end-effector.

2.2. Modeling of Joint Substructures

In this section, we will use the virtual joint method [34] to develop the model of a joint substructure. A joint substructure here is defined as an elastic system comprising one or more serially connected joint elements as shown in Fig.4, and each joint element corresponds to a 1-DOF joint, either a revolute or a prismatic joint. For example, a universal joint can be visualized as two serially connected revolute joints having orthogonal joints axes interacted at a common point. The same rule is applicable to a spherical joint.

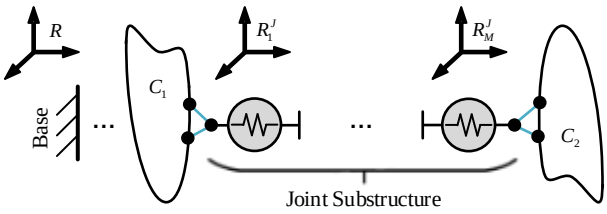

Fig.4 Joint substructure comprising serial connected springs

In order to evaluate compliances of a joint element numbered by $m\left(m = 1, \ldots, M, 1 \le M \le 3\right)$ in a joint substructure, place a body-fixed frame R_m^J attached to one of two parts of the joint element as shown in Fig.4. Note that R_m^J is set in such a way that one of its axis is aligned with the joint axis and all R_m^Js share the same origin. Then, the stiffness matrix of the joint substructure evaluated in R can be formulated as

$$\boldsymbol{k}^J = \left(\sum_{m=1}^{M} \boldsymbol{T}_{J,m} \boldsymbol{k}_m^{-1} \boldsymbol{T}_{J,m}^{\mathrm{T}} \right)^{-1} \tag{12}$$

where $\boldsymbol{k}_m$ is $n \times n$ stiffness matrix of the joint element m evaluated in R_m^J. If the element is a 1-DOF actuated joint, $n = 6$ and $\boldsymbol{T}_{J,m}$ has the form.

$$\boldsymbol{T}_{J,m} = \begin{bmatrix} \boldsymbol{R}_{J,m} & \boldsymbol{0} \\ \boldsymbol{0} & \boldsymbol{R}_{J,m} \end{bmatrix} \tag{13}$$

where $\boldsymbol{R}_{J,m}$ denotes the orientation matrix of R_m^J with respect to R. If, however, the element is a 1-DOF passive joint, a reduced form of the stiffness matrix with $n=5$ that covers only the constrained axes should be used. Meanwhile, the $\boldsymbol{T}_{J,m}$ given in Eq.(13) must be reduced by removing its column corresponding to the rigid body motion along/about the free axis, so giving a 6×5 matrix compatible with the reduced stiffness matrix. $\boldsymbol{k}_m$ can be modeled by a $n-$DOF virtual spring that gives diagonal entries. In this way, the nodal force, nodal displacement vectors and stiffness matrix of a 2-node joint substructure evaluated in R can be formulated by

$$\boldsymbol{F}^J = \boldsymbol{K}^J\boldsymbol{U}^J \quad \text{with} \quad \boldsymbol{F}^J = \begin{pmatrix} \boldsymbol{F}_1^J \\ \boldsymbol{F}_2^J \end{pmatrix}, \quad \boldsymbol{U}^J = \begin{pmatrix} \boldsymbol{U}_1^J \\ \boldsymbol{U}_2^J \end{pmatrix}, \quad \boldsymbol{K}^J = \begin{bmatrix} \boldsymbol{k}^J & -\boldsymbol{k}^J \\ -\boldsymbol{k}^J & \boldsymbol{k}^J \end{bmatrix} \tag{14}$$

2.3. Synthesis of Substructures

Equipped with the models of component substructures and joint substructures to hand, we proposed a procedure to synthesize the equations of motion of two arbitrary component substructures C_1 and C_2 connected by a joint substructure J as shown in Fig.5. Evaluated in R, the undamped equation of motion of substructure C_i developed by Eq.(11) can be represented by

$$\boldsymbol{M}_i^C\ddot{\boldsymbol{U}}_i^C + \boldsymbol{K}_i^C\boldsymbol{U}_i^C = \boldsymbol{F}_i^C, \quad i=1,2 \tag{15}$$

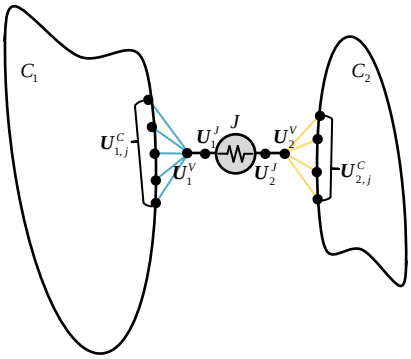

Fig.5 Different substructures assembled by enforcing continuity constraints

where $\boldsymbol{U}_i^C = \left(\left(\boldsymbol{U}_{i,j}^C\right)^{\mathrm{T}} \quad \left(\boldsymbol{U}_{i,p}^C\right)^{\mathrm{T}}\right)^{\mathrm{T}}$ with $\boldsymbol{U}_{i,j}^C$ being the junction displacement nodal vector and the internal elastic modal coordinate vector $\boldsymbol{U}_{i,p}^C$. In order to facilitate the substructure synthesis, we classify the junction surfaces into two types, associated respectively with revolute joint and prismatic joint. It can be seen from Fig.6(a) that for a revolute joint, the set of junction surface nodes participating the substructure synthesis remains unchanged. The same rule is applicable to a universal and a spherical joint. Whereas for a prismatic joint the above set on the junction surface varies with system configurations as shown in Fig.6(b). Therefore, it is necessary to retain the entire set of nodal displacements along the direction of a prismatic joint within its stroke such that a proper subset can be selected via inverse kinematics in the substructure synthesis at a given configuration.

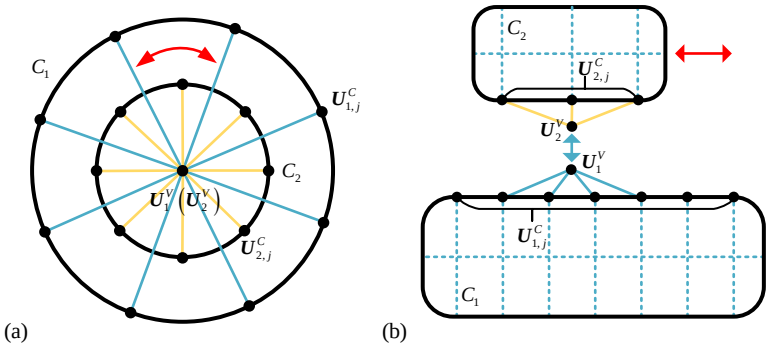

Fig.6 Two types of junction surface on component substructures

In order to force the nodal displacements on the junction surface of component substructure C_i to be compatible with the corresponding nodal displacement of joint substructure J, generate a 6-DOF virtual node that is attached to the component substructure C_i with its nodal displacement vector being $\boldsymbol{U}_i^V = \left(\boldsymbol{\varepsilon}_i^{\mathrm{T}} \quad \boldsymbol{\xi}_i^{\mathrm{T}}\right)^{\mathrm{T}}$ such that

$$\boldsymbol{U}_i^V - \boldsymbol{U}_i^J = \boldsymbol{0} \quad , i = 1,2 \tag{16}$$

where $\boldsymbol{\varepsilon}_i$ and $\boldsymbol{\xi}_i$ represent the translational and angular nodal displacement vectors of the virtual node，which can be determined by the weighted averaging interpolation method [35].

$$\boldsymbol{\varepsilon}_i = \frac{\sum_{q=1}^{f} w_{i,q} \boldsymbol{U}_{i,j,q}^C}{\sum_{q=1}^{f} w_{i,q}}, \quad \boldsymbol{\xi}_i = \frac{\sum_{q=1}^{f} w_{i,q} \left[\boldsymbol{r}_{i,q} \times\right] \boldsymbol{U}_{i,j,q}^C}{\sum_{q=1}^{f} w_{i,q} \left|\boldsymbol{r}_{i,q}\right|^2} \tag{17}$$

where $\boldsymbol{U}_{i,j,q}^C$ denotes the displacement vector of the qth$\left(q = 1,\ldots, f\right)$ junction node with f being the total number of junction nodes involved, $\boldsymbol{r}_{i,q}$ denotes the position vector pointing from the virtual node to the qth junction node，$\left[\boldsymbol{r}_{i,q} \times\right]$ is the skew matrix of $\boldsymbol{r}_{i,q}$, and $w_{i,q}$ is the weight factor proportional to the portion of the junction surface in order to ensure that the average sliding motion of the junction surface can be approximately represented by that of the virtual node.

Hence, rewrite Eq.(17) in matrix form leads to

$$\boldsymbol{U}_i^V = \begin{bmatrix} \dfrac{w_{i,1}\boldsymbol{I}_3}{\sum_{q=1}^{f} w_{i,q}} & \cdots & \dfrac{w_{i,q}\boldsymbol{I}_3}{\sum_{q=1}^{f} w_{i,q}} & \cdots & \dfrac{w_{i,f}\boldsymbol{I}_3}{\sum_{q=1}^{f} w_{i,q}} \\ \dfrac{w_{i,1}\left[\boldsymbol{r}_{i,1} \times\right]}{\sum_{q=1}^{f} w_{i,q} \left|\boldsymbol{r}_{i,q}\right|^2} & \cdots & \dfrac{w_{i,q}\left[\boldsymbol{r}_{i,q} \times\right]}{\sum_{q=1}^{f} w_{i,q} \left|\boldsymbol{r}_{i,q}\right|^2} & \cdots & \dfrac{w_{i,f}\left[\boldsymbol{r}_{i,f} \times\right]}{\sum_{q=1}^{f} w_{i,q} \left|\boldsymbol{r}_{i,q}\right|^2} \end{bmatrix} \begin{pmatrix} \boldsymbol{U}_{i,j,1}^C \\ \vdots \\ \boldsymbol{U}_{i,j,q}^C \\ \vdots \\ \boldsymbol{U}_{i,j,f}^C \end{pmatrix} = \boldsymbol{C}_i^V \boldsymbol{U}_{i,j}^C \tag{18}$$

where $\boldsymbol{I}_3$ is a unit matrix of order three. Substituting Eq.(18) into Eq.(16) yields the compatibility conditions of the component substructures C_1 and C_2 with the joint substructure J in between.

$$\boldsymbol{C}\boldsymbol{U} = \boldsymbol{0} \tag{19}$$

$$\boldsymbol{C} = \begin{bmatrix} \boldsymbol{C}_1^C & \boldsymbol{C}_2^C & \boldsymbol{C}^J \end{bmatrix}, \ \boldsymbol{C}_1^C = \begin{bmatrix} \boldsymbol{C}_1^V & \boldsymbol{0} \\ \boldsymbol{0} & \boldsymbol{0} \end{bmatrix}, \ \boldsymbol{C}_2^C = \begin{bmatrix} \boldsymbol{0} & \boldsymbol{0} \\ \boldsymbol{C}_2^V & \boldsymbol{0} \end{bmatrix}, \ \boldsymbol{C}^J = \begin{bmatrix} \boldsymbol{I}_6 & \boldsymbol{0} \\ \boldsymbol{0} & \boldsymbol{I}_6 \end{bmatrix}, \ \boldsymbol{U} = \begin{pmatrix} \boldsymbol{U}_1^C \\ \boldsymbol{U}_2^C \\ \boldsymbol{U}^J \end{pmatrix}$$

where $\boldsymbol{C}_i^C$ ($i = 1,2$) and $\boldsymbol{C}^J$ are defined as the nodal displacement operators for the component substructures C_i and joint substructure J, respectively.

In order to formulate the equation of the motion of the system composed of component substructures C_1, C_2 and joint substructure J, merge Eq.(14) and Eq.(15) into a compact form

$$\boldsymbol{M}\ddot{\boldsymbol{U}} + \boldsymbol{K}\boldsymbol{U} = \boldsymbol{F} \tag{20}$$

$$\boldsymbol{M} = \begin{bmatrix} \boldsymbol{M}_1^C & & \\ & \boldsymbol{M}_2^C & \\ & & \boldsymbol{0} \end{bmatrix}, \ \boldsymbol{K} = \begin{bmatrix} \boldsymbol{K}_1^C & & \\ & \boldsymbol{K}_2^C & \\ & & \boldsymbol{K}^J \end{bmatrix}, \ \boldsymbol{F} = \begin{pmatrix} \boldsymbol{F}_1^C \\ \boldsymbol{F}_2^C \\ \boldsymbol{F}^J \end{pmatrix}$$

where $\boldsymbol{M}$ and $\boldsymbol{K}$ are the mass and stiffness matrices of the unconstrained system, and $\boldsymbol{F}$ is the set of the nodal force vector imposed upon the junction surfaces. The formulation of Eq.(20) allows the equations of motion of the synthesized system to be achieved by using Lagrange multiplier method [36]

$$\begin{bmatrix} \boldsymbol{M} & \boldsymbol{0} \\ \boldsymbol{0} & \boldsymbol{0} \end{bmatrix} \begin{pmatrix} \ddot{\boldsymbol{U}} \\ \ddot{\boldsymbol{\lambda}} \end{pmatrix} + \begin{bmatrix} \boldsymbol{K} & \boldsymbol{C}^{\mathrm{T}} \\ \boldsymbol{C} & \boldsymbol{0} \end{bmatrix} \begin{pmatrix} \boldsymbol{U} \\ \boldsymbol{\lambda} \end{pmatrix} = \begin{pmatrix} \boldsymbol{F} \\ \boldsymbol{0} \end{pmatrix} \tag{21}$$

subject to $\boldsymbol{\lambda}^{\mathrm{T}}\boldsymbol{C}\boldsymbol{U} = \boldsymbol{0}$ with $\boldsymbol{\lambda} = \left(\lambda_1 \quad \cdots \quad \lambda_{12}\right)^{\mathrm{T}}$.

The equations of motion developed in Eq.(21) can be extended with ease to formulate those of a limb within a PKM system by properly numbering the component and joint substructures within the limb, leading to the equations of

motion of the parallel mechanism first by imposing loop closure compatibility conditions upon the platform and limbs using the Lagrange multiplier method. This can be followed by the formulation of equations of motion of a PKM having hybrid architecture using the same technique as illustrated by the example given in Section 3.

3. An Example

In this section, the elastodynamic model of a 5-DOF hybrid robot, named TriMule as shown in Fig.7, is established to illustrate the generality and effectiveness of the proposed approach. The hybrid robot is composed of an overconstrained 1T2R (T-translation, R-rotation) parallel mechanism and an A/C wrist. The parallel mechanism comprises a base, a platform, a base link, two identical RPS limbs, a UPS limb and a RP limb. Here, R, P, U, and S denote revolute, prismatic, universal, and spherical joints respectively, and the underlined P denotes an actuated prismatic joint.

Fig.8 shows the schematic diagram of the robot. Let B and B_i ($i=2,3$) be the centers of R joint connecting the RP limb and the ith RPS limb to the base link, and B_1 be the center of the U joint of the UPS limb; A_i ($i=1,2,3$) be the centers of the S joint connecting the UPS and RPS limbs to the RP limb, and A be the intersection of the axial axis of the RP limb with its normal plane in which all A_i are placed. A global reference frame R is attached to the point B with its z-axis normal to the plane of $\Delta B_1B_2B_3$ and its x-axis coincident with $\overline{B_2B_3}$. Firstly, the robot system is divided into four limbs, i.e., UPS limb numbered by 1, two RPS limbs numbered by 2 and 3 respectively and RP limb numbered by 4. Then, each limb is divided into different component substructures. Note that the wrist is serially connected with the platform which is rigidly connected with the RP limb, both of them are regarded as part of the RP limb. Meanwhile, it can be seen that the RP limb and two RPS limbs share the base link. For convenience, the base link is regarded as part of RP limb as well. There are twelve component substructures at all in this hybrid robot (see Table 1), i.e., (i) the outer ring of the U joint in limb 1, (ii) the wiggle link with screw in limb i ($i=1,2,3$), (iii) the telescopic link in limb i ($i=1,2,3$), (iv) the base link in limb 4, (v) the inner ring of passive limb in limb 4, (vi) the platform combined with the sliding part of passive limb in limb 4, (vii) the wrist, and (viii) the spindle in limb 4. The definitions of body-fixed frames are presented in Table 1.

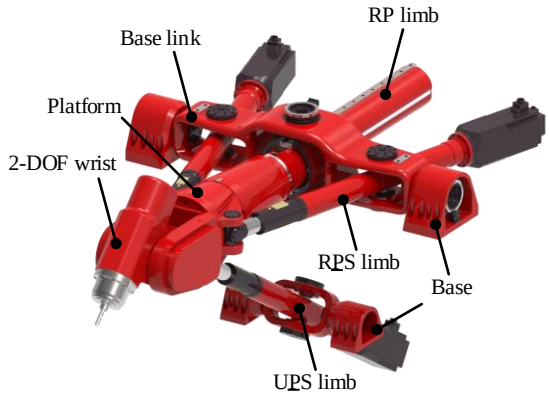

Fig.7 CAD model of the TriMule robot

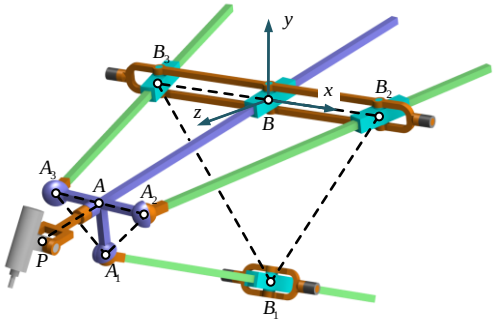

Fig.8 Schematic diagram of the TriMule robot

For each component substructure, FE model is generated from its CAD model using 10-noded solid tetrahedron element with density of 7800 kg/m^3, modulus of elasticity of 210 Gpa and Poisson's ratio of 0.28. For convenience, the significant component modes p for each substructure are set to 15 identically because this research is mainly focused on the low order natural frequencies of the hybrid robot. The junction DOFs for each component substructure represent the surface that contacts with joint substructures. By using the ICMS method introduced in section 2.1, the reduced system matrices of component substructures are constructed in their body-fixed frame according to the junction DOFs. Subsequently, the reduced models are transformed into the global reference frame. The DOFs of reduced model and full model for each component substructure are listed in Table 1.

Joint substructures in this robot include three identical R joints in RPS limbs, a R joint between the outer ring of the U joint and the base, two identical R joints between the base link and the base, three identical actuated P joints, three identical S joints, a R joint and a P joint in RP limb, and two different actuated R joints in the wrist. All the joint substructures comprise only one joint element in this robot except for three S joint substructures. Each S joint substructure comprises three serially connected 1-DOF joint elements. The system matrices of those joint substructures can be finally generated by the method proposed in section 2.2 and transformed into the global reference frame. The detailed stiffness parameters of those 1-DOF joint elements in joint substructure $t(t=1,\ldots,16)$ are given by product catalogues and handbooks or generated from FEA software, which are listed in Tables 2-4.

Table 1 Definitions of body-fixed frames and DOFs of component substructures

	R^C	Degrees of freedom	
		Full order model	Reduced model
i	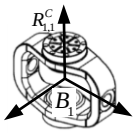	2820	297
ii	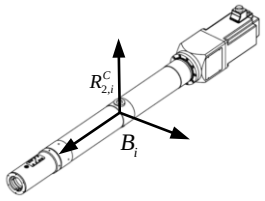	4791	561
iii	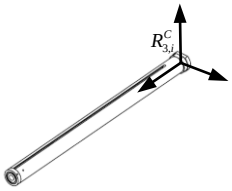	2142	186
iv	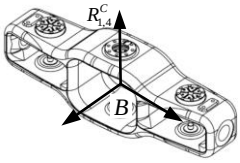	14391	1251
v	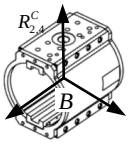	2658	276
vi	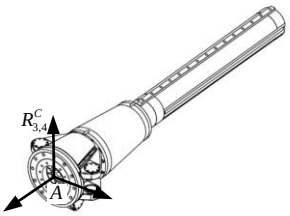	14673	1431
vii	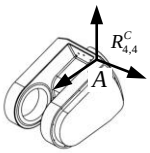	7653	744
viii	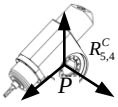	5442	477

To synthesize different substructures with incompatible displacement, virtual condensation nodes are established at the center of each junction surfaces using Eq.(16). The whole system is constrained by enforcing displacement compatibility condition between virtual node and corresponding node of joint substructure. Using Lagrange multiplier method, the undamped motion equation at a particular configuration of the robot is presented as

$$\boldsymbol{M}\ddot{\boldsymbol{U}} + \boldsymbol{K}\boldsymbol{U} = \boldsymbol{F} \tag{22}$$

where

$$\boldsymbol{M} = \mathrm{diag}(\boldsymbol{M}^C_{1,1}, \boldsymbol{M}^C_{2,1}, \boldsymbol{M}^C_{3,1}, \boldsymbol{M}^C_{2,2}, \boldsymbol{M}^C_{3,2}, \boldsymbol{M}^C_{2,3}, \boldsymbol{M}^C_{3,3}, \boldsymbol{M}^C_{1,4}, \boldsymbol{M}^C_{2,4}, \boldsymbol{M}^C_{3,4}, \boldsymbol{M}^C_{4,4}, \boldsymbol{M}^C_{5,4}, \boldsymbol{0}) \tag{23}$$

$$\boldsymbol{K} = \begin{bmatrix} \boldsymbol{K}' & \boldsymbol{C}^T \\ \boldsymbol{C} & \boldsymbol{0} \end{bmatrix} \tag{24}$$

$$\boldsymbol{K}' = \mathrm{diag}(\boldsymbol{K}_{1,1}^C, \boldsymbol{K}_{2,1}^C, \boldsymbol{K}_{3,1}^C, \boldsymbol{K}_{2,2}^C, \boldsymbol{K}_{3,2}^C, \boldsymbol{K}_{2,3}^C, \boldsymbol{K}_{3,3}^C, \boldsymbol{K}_{1,4}^C, \boldsymbol{K}_{2,4}^C, \boldsymbol{K}_{3,4}^C, \boldsymbol{K}_{4,4}^C, \boldsymbol{K}_{5,4}^C, \boldsymbol{K}^J) \tag{25}$$

$$\boldsymbol{K}^J = \mathrm{diag}(\boldsymbol{K}_1^J, \cdots, \boldsymbol{K}_t^J, \cdots, \boldsymbol{K}_{16}^J) \tag{26}$$

$$\boldsymbol{C} = \begin{bmatrix} \boldsymbol{C}_{1,1}^C & \boldsymbol{C}_{2,1}^C & \boldsymbol{C}_{3,1}^C & \boldsymbol{C}_{2,2}^C & \boldsymbol{C}_{3,2}^C & \boldsymbol{C}_{2,3}^C & \boldsymbol{C}_{3,3}^C & \boldsymbol{C}_{1,4}^C & \boldsymbol{C}_{2,4}^C & \boldsymbol{C}_{3,4}^C & \boldsymbol{C}_{4,4}^C & \boldsymbol{C}_{5,4}^C & \boldsymbol{C}^J \end{bmatrix} \tag{27}$$

and, $\left\{\boldsymbol{M}^C, \boldsymbol{K}^C\right\}$ are the reduced stiffness and mass matrices of corresponding component substructures, $\boldsymbol{K}_t^J$ is the stiffness matrix of corresponding joint substructure, $\boldsymbol{C}$ is a displacement operator coupling all substructures, $\boldsymbol{U}$ and $\boldsymbol{F}$ are the corresponding displacement vector and force vector, respectively.

Each time the configuration of the robot changes, the orientation transformation matrices for each substructure are determined by inverse kinematic analysis of the robot. The detailed inverse kinematic analysis process uses the same method as [37].

Table 2 Compliance matrices of different P joints

Type	$\boldsymbol{k}_{1,t}^{-1}$ (unit: N, m, rad)
Screw-nut assembly(actuated)	$\mathrm{diag}(3.29,1,1,5.16\times10^4,3.33\times10^3,3.33\times10^3)\times10^{-9}$
Guideway-slider assembly	$\mathrm{diag}(8,8,5.56\times10^4,3.51\times10^4,3.51\times10^4)\times10^{-9}$

Table 3 Compliance matrices of S joint substructure

m	Element of S joint	$\boldsymbol{k}_{m,t}^{-1}$ (unit: N, m, rad)
1	Short axis	$\mathrm{diag}(2.22,0.36,0.36,5\times10^4,5\times10^4)\times10^{-9}$
2	Long axis	$\mathrm{diag}(1.35,1.85,1.85,6.09\times10^3,6.09\times10^3)\times10^{-9}$
3	Cross axis	$\mathrm{diag}(3.39,0.42,0.42,5\times10^4,5\times10^4)\times10^{-9}$

Table 4 Compliance matrices of different R joints

The location of R joints	$\boldsymbol{k}_{1,t}^{-1}$ (unit: N, m, rad)
In RPS limb	$\mathrm{diag}(3.29,0.60,0.60,10^5,5\times10^5)\times10^{-9}$
Between the outer ring and the base	$\mathrm{diag}(1.65,0.37,0.37,5\times10^3,5\times10^3)\times10^{-9}$
Between the inner ring and the base link	$\mathrm{diag}(3.29,0.60,0.60,10^5,5\times10^5)\times10^{-9}$
Between the base link and the base	$\mathrm{diag}(0.8,0.15,0.15,333.33,333.33)\times10^{-9}$
Between the wrist and platform(actuated)	$\mathrm{diag}(5.88,1.18,1.18,2.97\times10^3,158.73,158.73)\times10^{-9}$
Between the spindle and wrist(actuated)	$\mathrm{diag}(1.05,2.27,2.27,2.60\times10^3,571.43,571.43)\times10^{-9}$

The static and dynamic analysis of the TriMule robot with the configuration changes over the workspace is made to verify the efficiency of the proposed modeling method. Let the reference point *P* of the robot at different positions of the middle plane of workspace (the circle plane when *z*=1125 mm, with *x*=0 mm, *y*=-200 mm as original point and *r*=600 mm as radius), the system dynamic formulation as Eq.(22) can be generated for each particular configuration. By applying unit force to the node placed point *P* in three directions *x*, *y* and *z*, the static stiffness of point *P* in corresponding directions can be solved. Fig.9 shows the distributions of the static stiffness of point *P* in the middle plane of the workspace calculated by the reduced model and by the full FE model using SAMCEF software respectively. By solving the eigenvalue problem of Eq.(22), Fig.10 shows the distributions of the first forth order natural frequencies of the robot in the middle plane of the workspace calculated by the reduced model and by the full FE model using SAMCEF software respectively.

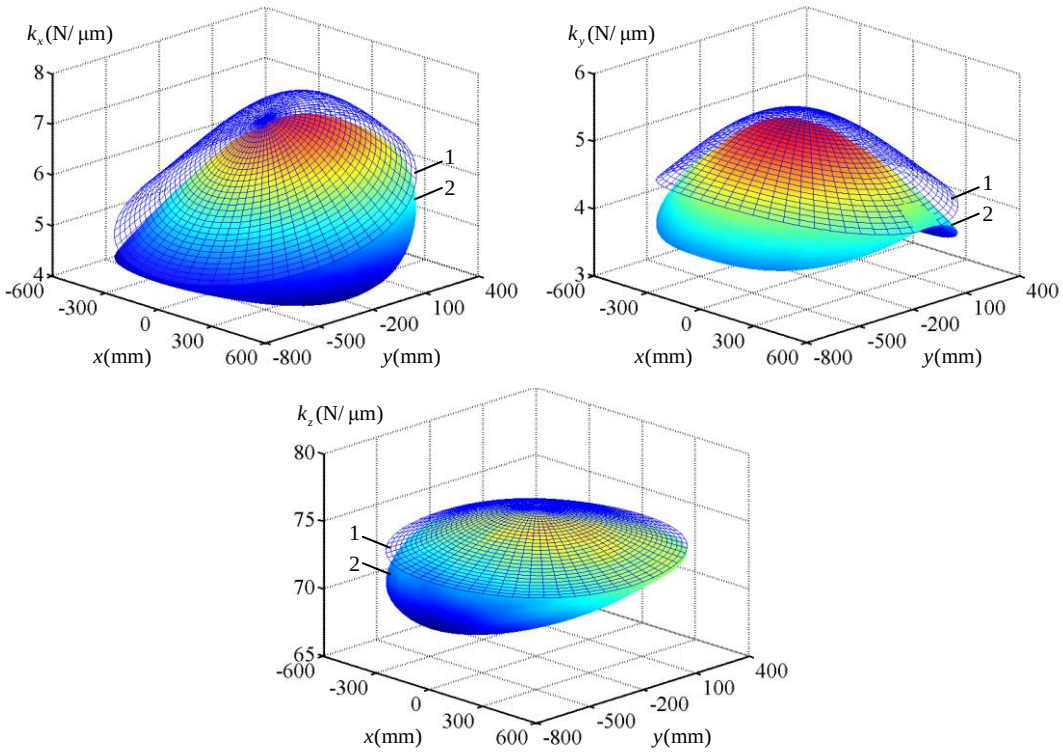

Fig.9 Static stiffness distributions in the middle plane of the workspace
1: Reduced model 2: Full model

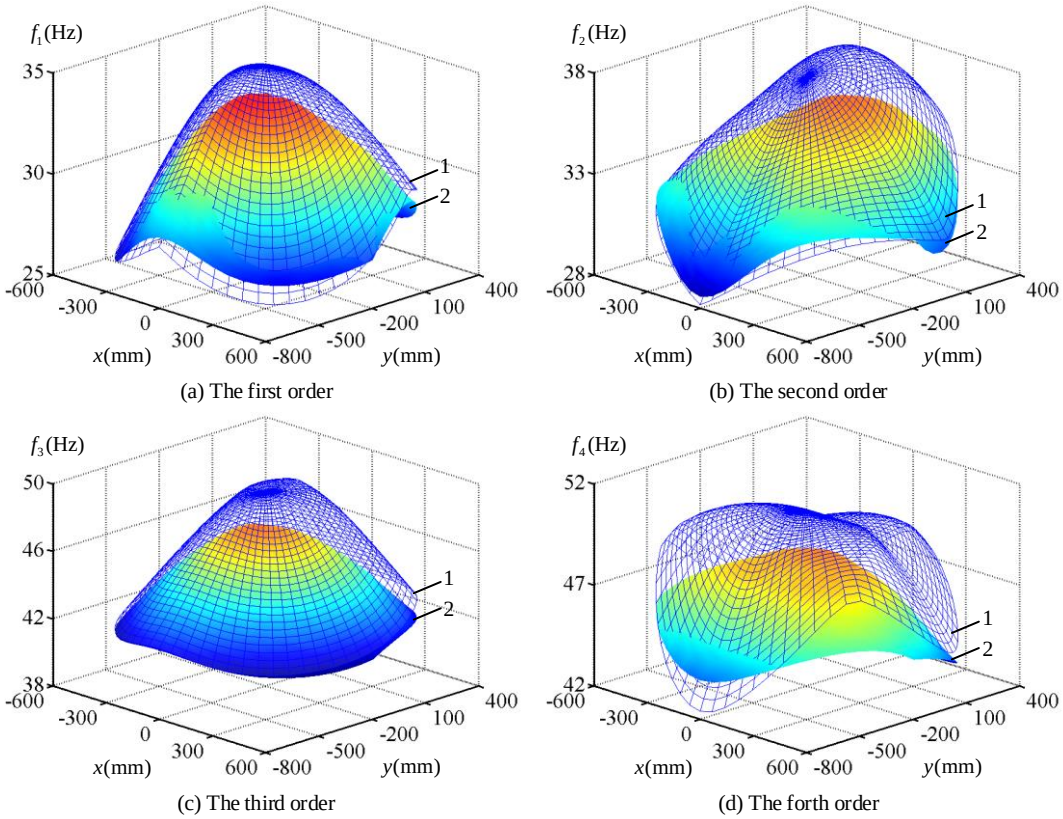

(a) The first order (b) The second order

(c) The third order (d) The forth order

Fig.10 The first forth order natural frequencies distributions in the middle plane of the workspace
1: Reduced model 2: Full model

As is evident, the static stiffness and natural frequency of the hybrid robot exhibit strong pose-dependency and the results obtained by the reduced model match satisfactorily those obtained by the full FE model according to

distributions. The distributions have the characteristic of plane symmetry, which coincides with the symmetry structure of the TriMule robot. It can be seen from Fig.9 that the maximum value of static stiffness along *x*-axis appears at *y*=0 mm in the symmetry plane, and along *y*-axis and *z*-axis appear at *y*=-200 mm. The value of static stiffness along three directions decrease monotonically from the symmetry plane to the boundary of the workspace, which means that the static performance of the robot is better in the symmetry plane than other positions. In addition, it can also be observed that the static stiffness along *y*-axis are slightly smaller than *x*-axis, while its values along *z*-axis are much greater. Therefore, more attention should be paid to the static stiffness along *x*-axis and *y*-axis in both the design phase and application phase. As for natural frequencies, it can be seen from Fig.10 that the maximum values of the first order and the second order natural frequencies appear at *y*=-200 mm and *y*=0 mm in the symmetry plane respectively. Similar to the static stiffness, the values of natural frequencies in the symmetry plane decrease monotonically towards the boundary of the workspace, which shows that the robot demonstrates better dynamic performance in the symmetry plane. To show the results clearly, Table 5 is given to compare the results at the specific configuration, where *x*=0 mm, *y*=-200 mm, and *z*=1125 mm. It can be seen the results obtained by the reduced model clearly match those of the full FE model in terms of magnitude, which further proves that the proposed model can depict the static and dynamic characteristics of the TriMule robot accurately. At the same time, just as shown in Table.1, the size of the proposed model is far less than the full FE model, which leads to less computation time. For a particular configuration, the modal analysis of the reduced model takes only about 45 seconds while the full FE model costs 125 seconds (Intel i5-4430CPU with 12GB RAM). In addition, the proposed approach is a kind of generalized methodology, which means that it can be utilized for depicting the static and dynamic characteristics of the robot with different topological architectures. Therefore, the proposed methodology lays a solid ground for the design, performance evaluation and cutting stability prediction of the industrial robots.

Table 5 Results obtained by the reduced model and the full FE model

	k_x(N/ μm)	k_y(N/ μm)	k_z(N/ μm)	f_1(Hz)	f_2(Hz)	f_3(Hz)	f_4(Hz)
The reduced model	7.09	5.47	75.98	35.28	37.71	49.43	50.53
The full FE model	6.70	5.27	73.39	33.68	35.50	47.49	48.11
Residual	5.82%	3.80%	3.53%	4.75%	6.23%	4.09%	5.03%

4. Conclusions

By combining substructure synthesis and modal reduction techniques with the virtual joint method, this paper introduces a general and systematic approach for elastodynamic modeling of parallel kinematic machines. The following conclusions are drawn.

(1) A generalized method for pose-dependency modeling of the PKMs is proposed based on substructure synthesis of reduced order models as an alternative to presently used, time consuming full FE models. Meanwhile, joints stiffness are taken into consideration by using 6-DOF virtual spring with stiffness coefficients obtained by product catalogues, handbooks or experimental measurements. To synthesize component substructures with joint substructures, interpolation multipoint constraint equation is used to establish virtual nodes satisfying displacement compatibility with nodes on joint substructures. Synthesized reduced model can be updated conveniently at any configuration of the PKMs for static and dynamic performances prediction.

(2) The effectiveness of the proposed approach has been confirmed by a comparison study against the FEA software. The results of stiffness and natural frequencies analysis of TriMule hybrid robot show that sufficient computational accuracy can be achieved while making huge computational time savings (over FEA) for the prediction of static and dynamic performances over the entire workspace. The proposed approach is therefore valuable in both design phase and application phase.

Acknowledgements

This research work was partially supported by National Natural Science Foundation of China (NSFC) under grant 51420105007 and EU H2020-RISE-ECSASDP (Grant 734272).

References

[1] Weck M, Staimer D. Parallel kinematic machine tools–current state and future potentials[J]. CIRP Annals-Manufacturing Technology, 2002, 51(2): 671-683.

[2] Tlusty J, Ziegert J, Ridgeway S. Fundamental comparison of the use of serial and parallel kinematics for machines tools[J]. CIRP Annals-Manufacturing Technology, 1999, 48(1): 351-356.

[3] Xu Y, Zhang D, Yao J, et al. Type synthesis of the 2R1T parallel mechanism with two continuous rotational axes and study on the principle of its motion decoupling[J]. Mechanism and Machine Theory, 2017, 108: 27-40.

[4] Wang L, Xu H, Guan L. Optimal design of a 3-PUU parallel mechanism with 2R1T DOFs[J]. Mechanism and Machine Theory, 2017, 114: 190-203.

[5] Liu H, Huang T, Kecskeméthy A, et al. Force/motion transmissibility analyses of redundantly actuated and overconstrained parallel manipulators[J]. Mechanism and Machine Theory, 2017, 109: 126-138.

[6] Xie F, Liu X J, Luo X, et al. Mobility, Singularity, and Kinematics Analyses of a Novel Spatial Parallel Mechanism[J]. Journal of Mechanisms and Robotics, 2016, 8(6): 061022.
[7] Assal S F M. A novel planar parallel manipulator with high orientation capability for a hybrid machine tool: kinematics, dimensional synthesis and performance evaluation[J]. Robotica, 2015, 35(5):1031-1053.
[8] Xie F, Liu X J, Wang J. A 3-DOF parallel manufacturing module and its kinematic optimization[J]. Robotics and Computer-Integrated Manufacturing, 2012, 28(3): 334-343.
[9] Xie F, Liu X J. Analysis of the kinematic characteristics of a high-speed parallel robot with Schönflies motion: Mobility, kinematics, and singularity[J]. Frontiers of Mechanical Engineering, 2016, 11(2): 135-143.
[10] Zhang D, Xu Y, Yao J, et al. Kinematics, dynamics and stiffness analysis of a novel 3-DOF kinematically/actuation redundant planar parallel mechanism[J]. Mechanism and Machine Theory, 2017, 116: 203-219.
[11] Wu J, Li T, Wang J, et al. Stiffness and natural frequency of a 3-DOF parallel manipulator with consideration of additional leg candidates[J]. Robotics and Autonomous Systems, 2013, 61(8): 868-875.
[12] Bianchi G, Tosatti L M, Fassi I. Virtual prototyping of parallel mechanisms[J]. Proceedings of the Institution of Mechanical Engineers, Part K: Journal of Multi-body Dynamics, 2002, 216(1): 21-37.
[13] Altintas Y, Brecher C, Weck M, et al. Virtual machine tool[J]. CIRP Annals-manufacturing technology, 2005, 54(2): 115-138.
[14] Zhang D, Wang L, Lang S Y. Parallel kinematic machines: design, analysis and simulation in an integrated virtual environment[J]. Journal of Mechanical Design, 2005, 127(4): 580-588.
[15] Ma Y, Niu W, Luo Z, et al. Static and dynamic performance evaluation of a 3-DOF spindle head using CAD–CAE integration methodology[J]. Robotics and Computer-Integrated Manufacturing, 2016, 41: 1-12.
[16] Book W J. Recursive Lagrangian dynamics of flexible manipulator arms[J]. The International Journal of Robotics Research, 1984, 3(3): 87-101.
[17] Sunada W H, Dubowsky S. On the dynamic analysis and behavior of industrial robotic manipulators with elastic members[J]. Journal of Mechanisms, Transmissions, and Automation in Design, 1983, 105(1): 42-51.
[18] Kovecses J. A Distributed Parameter Model for the Dynamics of Flexible-Link Robots[J]. J. Robotic Systems, 1998, 15(5): 281-298.
[19] Li H, Yang Z, Huang T. Dynamics and elasto-dynamics optimization of a 2-DOF planar parallel pick-and-place robot with flexible links[J]. Structural and Multidisciplinary Optimization, 2009, 38(2): 195-204.
[20] Piras G, Cleghorn W L, Mills J K. Dynamic finite-element analysis of a planar high-speed, high-precision parallel manipulator with flexible links[J]. Mechanism and machine theory, 2005, 40(7): 849-862.
[21] Zhou Z, Xi J, Mechefske C K. Modeling of a fully flexible 3PRS manipulator for vibration analysis[J]. Journal of Mechanical Design, 2006, 128(2): 403-412.
[22] Fattah A, Angeles J, Misra A K. Dynamics of a 3-DOF spatial parallel manipulator with flexible links[C]//Robotics and Automation, 1995. Proceedings., 1995 IEEE International Conference on. IEEE, 1995, 1: 627-633.
[23] Wang X, Mills J K. Dynamic modeling of a flexible-link planar parallel platform using a substructuring approach[J]. Mechanism and machine theory, 2006, 41(6): 671-687.
[24] Craig R R. Structural dynamics: an introduction to computer methods [M]. John Wiley & Sons Inc, 1981.
[25] Liew K M, Leek S E, Liu A Q. Mixed-interface substructures for dynamic analysis of flexible multibody systems[J]. Engineering structures, 1996, 18(7): 495-503.
[26] Wu H T, Mani N K, Ashrafiuon H. Selection of modal basis for flexible bodies of mechanical systems[J]. Mechanism and machine theory, 1995, 30(3): 471-489.
[27] Law M, Ihlenfeldt S, Wabner M, et al. Position-dependent dynamics and stability of serial-parallel kinematic machines[J]. CIRP Annals-Manufacturing Technology, 2013, 62(1): 375-378.
[28] T. Huang, C. Dong, H. Liu, X. Qin, J. Mei, Q. Liu, M. Wang, "Five-degree-of-freedom Parallel Robot with Multi-shaft Rotary Brackets," Pub. No.: WO/2017/005015, 2017-01-12.
[29] Farhat C, Geradin M. On a component mode synthesis method and its application to incompatible substructures[J]. Computers & Structures, 1994, 51(5): 459-473.
[30] Craig R, Bampton M. Coupling of substructures for dynamic analyses[J]. AIAA journal, 1968, 6(7): 1313-1319.
[31] Guyan R J. Reduction of stiffness and mass matrices[J]. AIAA journal, 1965, 3(2): 380.
[32] Friswell M I, Garvey S D, Penny J E T. Model reduction using dynamic and iterated IRS techniques[J]. Journal of sound and vibration, 1995, 186(2): 311-323.
[33] Masson G, Brik B A, Cogan S, et al. Component mode synthesis (CMS) based on an enriched Ritz approach for efficient structural optimization[J]. Journal of sound and vibration, 2006, 296(4): 845-860.
[34] Liu H, Huang T, Chetwynd D G, et al. Stiffness Modeling of Parallel Mechanisms at Limb and Joint/Link Levels[J]. IEEE Transactions on Robotics, 2017, 33(3):734-741.
[35] Heirman G H K, Desmet W. Interface reduction of flexible bodies for efficient modeling of body flexibility in multibody dynamics[J]. Multibody System Dynamics, 2010, 24(2): 219-234.
[36] Liu G R, Quek S S. The finite element method: A practical course[M]// The finite element method : a practical course. Butterworth-Heinemann, 2003.
[37] Li M, Huang T, Mei J, et al. Dynamic formulation and performance comparison of the 3-DOF modules of two reconfigurable PKM—the Tricept and the TriVariant[J]. Journal of Mechanical Design, 2005, 127(6): 1129-1136.